# Observation and Optical Tailoring of Photonic Lattice Filaments

M. Bellec,[1] P. Panagiotopoulos,[1] D. G. Papazoglou,[1,2] N. K. Efremidis,[3] A. Couairon,[4] and S. Tzortzakis[1,2]

[1]*Institute of Electronic Structure and Laser, Foundation for Research and Technology Hellas, P.O. Box 1527, 71110 Heraklion, Greece*
[2]*Department of Materials Science and Technology, University of Crete, P.O. Box 2208, GR-71003 Heraklion, Greece*
[3]*Department of Applied Mathematics, University of Crete, P.O. Box 2208, GR-71003 Heraklion, Greece*
[4]*Centre de Physique Théorique, Centre National de la Recherche Scientique, Ecole Polytechnique, F-91128 Palaiseau, France*

(Received 22 July 2011; revised manuscript received 4 May 2012; published 14 September 2012)

We demonstrate, for the first time, that photonic lattices support a new type of laser filaments, called lattice filaments (LF). The LF attributes (length, width, and intensity) can be tailored by both varying the photonic lattice properties and also dynamically through the interaction between filaments. This opens the way for extensive all-optical control of the nonlinear propagation of intense ultrafast wave packets. Our approach is generic and applicable to all transparent media, with potential strong impact on various photonic applications.

DOI: 10.1103/PhysRevLett.109.113905 PACS numbers: 42.25.Bs, 05.45.Yv, 42.65.Jx, 42.65.Re

Laser filaments are wave packets with an intense peak interacting with the propagation medium over long distances. In bulk media, first observations of long pulse filamentation were understood as a manifestation of light self-trapping, often associated with material damage [1]. Later, ultrashort laser pulse filamentation in air was demonstrated in Ref. [2] and has attracted a growing interest in both fundamental and applied fields, ranging from single-cycle pulse generation [3] to electric discharge triggering and guiding [4], remote sensing and atmospheric water condensation [5], and THz generation [6]. Filaments appear at laser pulse powers exceeding a critical power, $P_{cr}$, and result from a competition involving the optical Kerr effect, generation of free electrons, plasma-induced defocusing, nonlinear losses and dispersion [7]. A control of this competition is extremely challenging since specific applications of filaments would request some of their features to be tuned along the propagation distance. For instance, micromachining of optical media in the bulk with filaments would highly benefit from tunability of the diameter, peak intensity, and depth of the filament. However, high intensities within a standard filament make this task almost impossible with conventional optical elements. Up to now, the majority of filamentation tailoring efforts are limited to the use of amplitude and phase masks [7,8], wave front aberrations [9], or temporal pulse shaping [10] for reshaping the laser beam or pulse before it undergoes filamentation. The filamentation dynamics, however, is barely modified by initial pulse reshaping, calling for new methods for extensive control of the filament attributes. Recently, we demonstrated by means of numerical simulations that the techniques for stabilizing spatial solitons via the use of photonic lattices [11,12] extend advantageously to filamentation control [13]. We showed that the temporal dynamics of a self-induced filament (SF) is quenched by sending the laser pulse in a lattice of reduced refractive index generated by plasma in air. Diffraction due to the lattice modifies the competition between linear and nonlinear effects that occur in a SF. It prevents high intensities from being reached, thereby limiting nonlinear losses, by regularizing the energy flux from the periphery to the core of the filament. A nonlinear structure called intense lattice filament (LF) forms over a short propagation distance in the lattice, with attributes that can be effectively tailored by adjusting the lattice properties (modulation depth and period).

In this Letter, we extend this idea to lattices in solid media. We present the first experimental realization of LFs and show that the LF properties can indeed be tailored. We demonstrate that a LF can be refilled in energy by interaction with a filament, opening the way to remote replenishment of filaments.

For our experiments, we fabricated photonic lattices in BK7 glass using the femtosecond laser writing technique [14]. Our lattice consists of seven periodically arranged waveguides 24 mm long, spaced by 25 $\mu$m with an elliptical cross section ($5 \times 25$ $\mu$m); see inset in Fig. 1(c). The refractive index modification is negative and is estimated to be $\Delta n \sim -10^{-4}$. Due to the high intensity of the filament [15], its propagation is accompanied by a nonlinear fluorescence emission [16]. This emission is laterally ($yz$ plane in Fig. 1) imaged on a linear CCD camera, using a 0.11 NA microscope objective and thus allowing the visualization of the nonlinear propagation. Since a nonlinear law correlates the fluorescence signal to the intensity, the image contrast and the intensity ratio between SF and LF are affected [14]. Figure 1 depicts both numerical and experimental results showing how the photonic lattice affects the propagation of the filament. In the presence of the lattice, the peak intensity drops and the filament length extends from 2 to 7 mm, giving rise to a LF.

To understand the experimental signature of the LF, the nonlinear propagation with and without the photonic lattice is numerically studied using an extended *stationary*

 

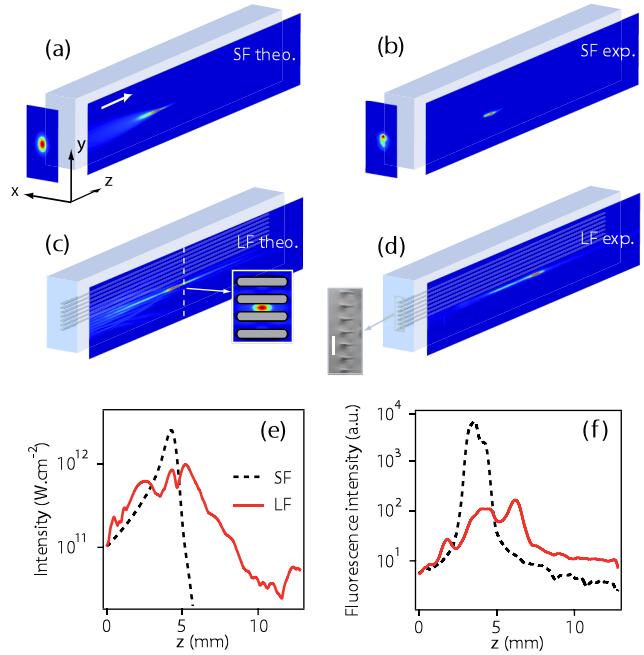


FIG. 1 (color online). (a) and (b) Simulated and experimental SF propagation ($yz$ plane). (c) and (d) Simulated and experimental LF propagation. The input is an 80 $\mu$m wide Gaussian beam ($xy$ plane). The white arrow indicates the light propagation direction. The photonic lattice parameters are $\Delta n = -4 \times 10^{-4}$, $\Lambda = 25$ $\mu$m, and $L = 24$ mm. For the simulation, the inset shows the elliptical cross section. For the experimental visualization, the emitted fluorescence is collected by imaging the $yz$ plane on a CCD camera. Note that the $yz$ images size is $0.4 \times 13$ mm. The inset shows a transverse view of the fs laser-induced structures. The white line corresponds to 30 $\mu$m. (e) and (f) Corresponding intensity profiles versus the propagation length.

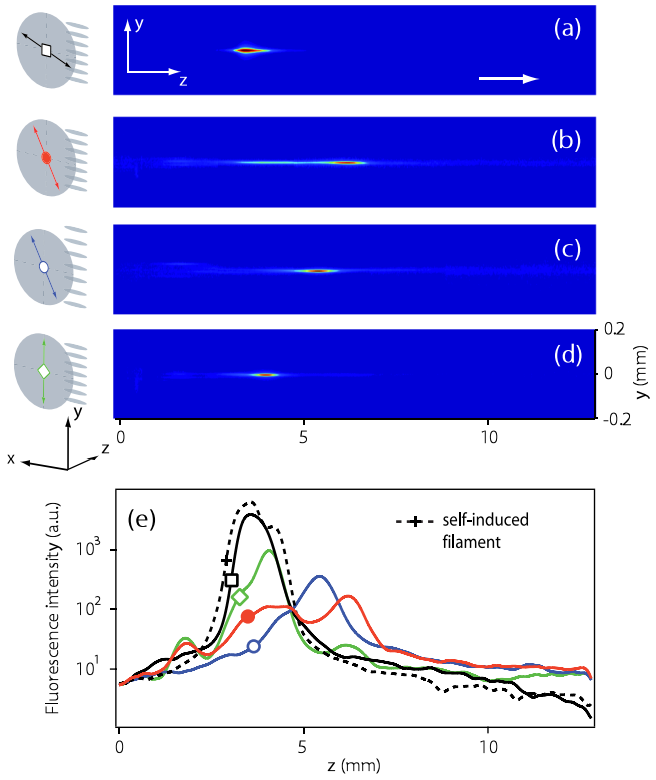


FIG. 2 (color online). Fluorescence images for different input polarization ($P$) and lattice period ($\Lambda$): (a) $P = 20°$, $\Lambda = 25$ $\mu$m; (b) $P = 60°$, $\Lambda = 25$ $\mu$m; (c) $P = 60°$, $\Lambda = 35$ $\mu$m; and (d) $P = 90°$, $\Lambda = 25$ $\mu$m. (e) Corresponding longitudinal profiles (in log scale) compared to the SF profile (gray dashed line).

nonlinear envelope equation accounting for the effects of Kerr nonlinearity, multiphoton absorption, and plasma defocusing. Details on the model used can be found in the Supplemental Material [17], and technical details on the resolution method used are given in Ref. [18]. The input laser pulse is a Gaussian beam centered at 800 nm with a beam waist of 80 $\mu$m and a pulse duration of 35 fs. The input power is 0.6 $\mu$J corresponding to $5P_{cr}$ (where $P_{cr} =$ 3.7 MW in BK7 [7]). An initial curvature corresponding to the effect of a 30 cm focal length lens is added to take into account the focusing. The model for the lattice reproduces the experimental lattice and particularly the elliptical cross section.

The inherent birefringence of the induced structures, a common side effect in laser structuring of glass, is exploited to fine-tune the LF attributes by rotating the input laser polarization (the optical properties of the birefringent lattice are a function of the input polarization orientation). A study of the effect of the input polarization $P$ and period $\Lambda$ on the propagation of the LF is presented in Fig. 2. For a given period ($\Lambda = 25$ $\mu$m), as the input polarization is rotated, the peak intensity drops, its distribution becomes more homogeneous and the propagation length is extended. The optimal configuration, in terms of length and uniformity, is achieved for $P = 60°$ [Fig. 2(b)]. Then, by further rotating the polarization, the beam is still elongated but is less uniform with an intense peak at 4 mm [Fig. 2(d)]. Similarly, at a given polarization state ($P = 60°$), when the lattice period is increased at 35 $\mu$m [Fig. 2(c)], the propagation length remains relatively long but a peak emerges at 5.5 mm, affecting the LF uniformity. As depicted in Fig. 3, the photonic lattice also affects the filament width and consequently the output power. Without lattice, the measured full width at half maximum of the SF is 5 $\mu$m (dashed line). The presence of the lattice leads to a clear widening up to 8.5 $\mu$m ($P = 60°$). The total losses encountered by the pulse during the propagation, as measured by the output power, are shown in Fig. 3(b). For input powers much smaller than $P_{cr}$, the intensity does not reach values where multiphoton absorption is important and the pulse propagates almost without losses (dashed line). By increase of the input power, nonlinear losses become more significant. For instance, for an input power of $5P_{cr}$, the losses can be as high as 25% for a SF. However, due to its larger width and consequently lower intensity, the LF

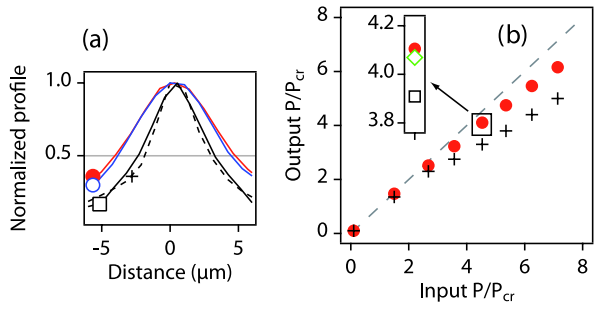


FIG. 3 (color online). (a) Transverse profile of the LF for various configurations ($P$ and $\Lambda$, see Fig. 2) compared to SF (dashed curve and crosses). (b) Power measured at the output of the glass sample for different input power for the LF (filled circles) and the SF (crosses). For BK7, $P_{cr} = 3.7$ MW. The gray dashed line represents the linear propagation regime (i.e., no losses). The inset shows the output power for $5P_{cr}$ input power in various configurations. The drop of the peak intensity and the increase of the propagation length is associated with a widening of the filament and, consequently, a more significant output power.

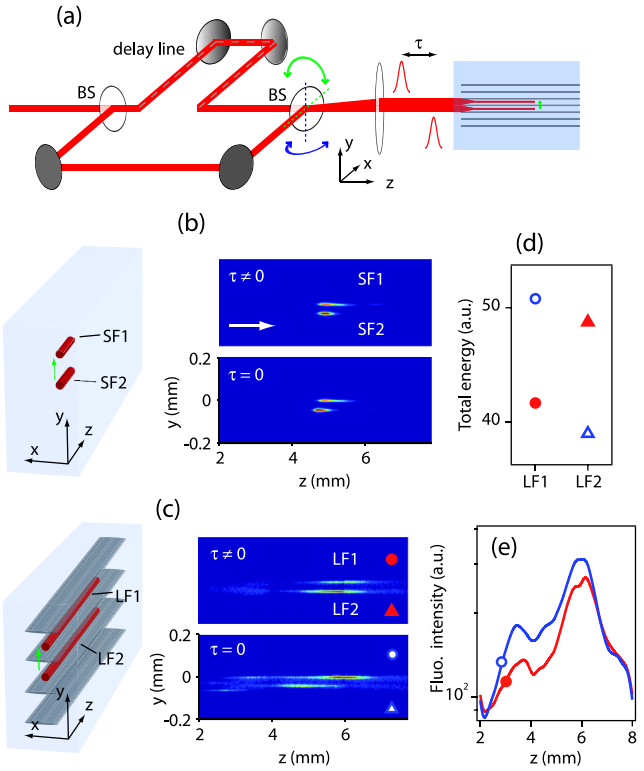


FIG. 4 (color online). (a) Experimental setup. A delay line is used to separate in time the two pulses. One of the beam splitters (BS) is slightly rotated either around the $x$ (green arrows) or the $y$ axis (blue arrows) to spatially separate the two filaments. (b) Two SFs (SF1 and SF2) spaced by 50 $\mu$m (green arrow) overlapped in time ($\tau = 0$, bottom) and not ($\tau \neq 0$, top). (c) Same as (b) for two LFs (LF1 and LF2). The top and the bottom filaments are labeled 1 and 2, respectively. The widening of the LF, waist increases the coupling and leads the two LFs to interact. (d) Total energy (integrated fluorescence intensity) of the LF1 (circles) and the LF2 (triangles) at both $\tau = 0$ (opened symbols) and $\tau \neq 0$ (filled symbols) cases. An energy transfer occurs from LF2 to LF1. (e) Longitudinal profiles of the LF1 for $\tau = 0$ (opened blue circle) and $\tau \neq 0$ (filled red circle) cases.

experiences weaker nonlinear losses during the propagation (10% at $5P_{cr}$). Thus, due to their tailored properties (intensity, propagation length, uniformity, and width), the formation of LFs also offers significantly lower losses, which makes them great candidates for applications such as pulse compression, etc.

In the following, the nonlinear nature of the lattice filaments is clearly demonstrated during their interaction. We explore the interaction between filaments in lattices and offer additional means of tailoring the LF attributes. We used the experimental setup presented in Fig 4(a) to separate two filaments both spatially and temporally. We study first the interaction between two LFs. As qualitative reference, we show in Fig. 4(b) the fluorescence images of two SFs (labeled SF1 and SF2) separated by 50 $\mu$m (along the $y$ axis, green arrow) that are either overlapped in time (i.e., zero time delay, $\tau = 0$) or not ($\tau \neq 0$). We clearly observe no interaction between the two SFs even when they are overlapped in time as expected for a separation distance that is larger than the typical interaction length of SFs [19]. Figure 4(c) shows the same experiment for two beams LFs [labeled LF1 and LF2; with $P = 60°$, $\Lambda = 35$ $\mu$m, same as Fig. 2(c)] that are also spatially separated by 50 $\mu$m. When the LFs are not overlapped in time. the image is equivalent to the addition of two independent LFs as expected if no interaction takes place. However, the situation is strikingly different when the two LFs are at zero time delay. Interaction is now clear. Indeed, due to their wider transverse distribution, compared to the SFs, there is coupling between the two LFs leading to an energy exchange. The total energy (integrated intensity) of the LF1 is shown in Fig. 4(d) and compared to the evolution of the total energy of the LF2. While the energy of LF1 increases by about 25%, the energy of LF2 drops by a similar quantity. A careful view of Fig. 4(b) shows that the maximum intensity of the 2 LFs is slightly different. The energy transfer occurs between the 2 LFs from the stronger to the less intense filament, LF2 and LF1 respectively. As plotted in Fig. 4(e) ($\tau = 0$ case) the energy transfer leads to a more intense LF. This behavior is also encountered during the interaction of solitons and filaments. Nonlinear interaction through the energy reservoir that sustains these structures leads to an energy exchange [7].

Next we investigated the interaction between a SF and a LF. The spacing between the two input beams is reduced to 20 $\mu$m in the $y$ direction. As sketched in Figs. 5(a) and 5(b), one beam is slightly shifted along the $x$ axis (blue arrow) to spatially place it out of the photonic lattice. Again, as a qualitative reference, we show in Fig. 5(a) the interaction of two SFs (SF1 and SF2), separated by 20 $\mu$m. In this case, the SFs are close enough to strongly interact when they are

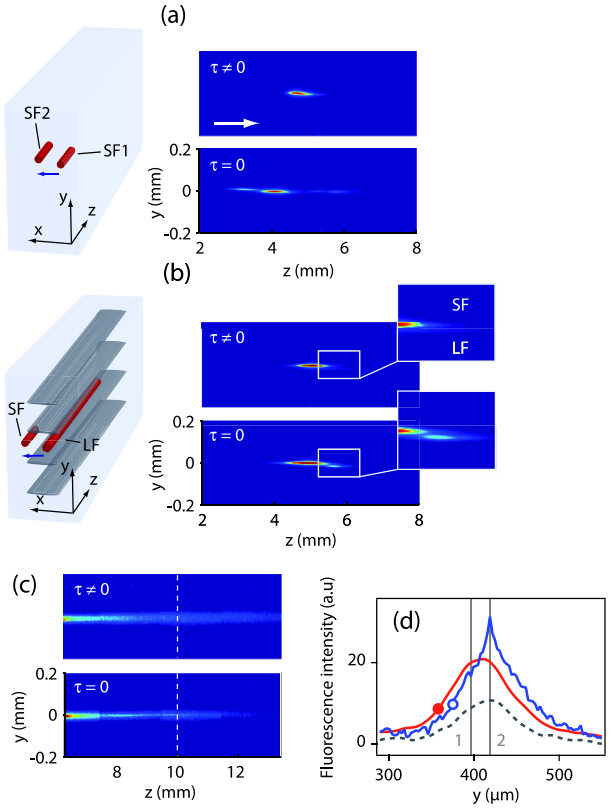


FIG. 5 (color online). (a) Two SFs (SF1 and SF2) spaced by 20 $\mu$m (blue arrow) overlapped in time ($\tau = 0$, bottom) and not ($\tau \neq 0$, top). (b) One SF and one LF at $\tau = 0$ (bottom) and $\tau \neq 0$ (top). The SF is obtained by slightly shifting the top beam (blue arrow) to be out of the photonic lattice. (c) Same as (b) for longer propagation length (from 6.5 to 13 mm). (d) Transversal profile at $z = 10$ mm [white line of (c)] of a single LF (dashed gray curve), of both the SF and LF at $\tau \neq 0$ (filled red circle) and of both the SF and LF at $\tau = 0$ (opened blue circle). The two gray lines represent the position of the SF (1) and the LF (2).

overlapped in time and merge to form an intense filament with its focus shifted towards the laser source. This configuration leads to an unstable propagation. On the other hand, in the presence of the photonic lattice [20], Fig. 5(b) shows that when the two pulses are not temporally overlapped the LF propagation is not affected by the presence of the SF. However, when they are at $\tau = 0$ (bottom image), the intensity of the LF is increased, a clear indication of energy transfer from the SF to the LF. The wider spatial profile of LFs enables them to interact with other nonlinear optical waves such as SF in favor of their energy. To better visualize this effect, we show in Fig. 5(c) the propagation of the LF for longer propagation distances (from 6 to 13 mm). The corresponding transverse profiles measured at a propagation distance $L = 10$ mm are plotted in Fig. 5(d). The dashed line represents the profile of a single LF (without the SF). At this distance, the LF is spatially broadened. In the presence of a SF at $\tau \neq 0$ (filled circle), the widened profile simply corresponds to the addition of two contributions: the single LF signal (centered at position 2, dashed curve) and the intense SF trace (centered at position 1, not shown). We observe that when the two filaments are at $\tau = 0$ (open circle), the LF is drastically affected by the presence of the SF. The propagation length of the LF is enhanced up to 11 mm leading to the sharp peak centered at position 2. The increased background corresponds to the SF signal. It is worth noting that this behavior is not observed when a single LF propagates with twice the initial power (i.e., 10 $P_{cr}$). In that case, though the amplitude is twice more intense, the distribution is similar to the initial LF. These results suggest that the SF acts as an energy reservoir for the LF [7], allowing a significant increase of its propagation length.

To summarize, we have shown the first experimental evidence of photonic lattice filaments in solid media, i.e., new type of filaments with some attributes belonging to solitons and others to self-induced filaments. Self-action effects, which dominate self-induced filamentation and exclude any remote control over the filament attributes, have been regulated by appropriately selecting the lattice properties. Likewise, the inherent birefringence of the lattice fabricated in glass has been exploited to fine-tune the lattice filament attributes by rotating the input polarization. We have also shown that, through a nonlinear interaction process, a second filament can be used as a virtual optical element to further tailor a lattice filament in respect to its intensity, uniformity, and propagation length. Since our results open up the way for all-optical control of the propagation of intense ultrafast wave packets, our approach is expected to have a significant impact not only on the technologies utilizing laser filaments but also on numerous photonic applications.

This work was supported by the European Union Marie Curie Excellence Grant MULTIRAD Grant No. MEXTCT-2006-042683. N. K. E. was partially supported by the FP7-REGPOT-2009-1 project Archimedes Center for Modeling, Analysis and Computation.

[1] R. G. Brewer, J. R. Lifsitz, E. Garmire, R. Y. Chiao, C. H. Townes, and Y. S. I. Cal, Phys. Rev. **166**, 326 (1968).
[2] A. Braun, G. Korn, X. Liu, D. Du, J. Squier, and G. Mourou, Opt. Lett. **20**, 73 (1995).
[3] H. S. Chakraborty, M. B. Gaarde, and A. Couairon, Opt. Lett. **31**, 3662 (2006); A. Couairon, M. Franco, A. Mysyrowicz, J. Biegert, and U. Keller, Opt. Lett. **30**, 2657 (2005).
[4] S. Tzortzakis, B. Prade, M. Franco, A. Mysyrowicz, S. Hüller, and P. Mora, Phys. Rev. E **64**, 057401 (2001).
[5] J. Kasparian, M. Rodriguez, G. Méjean, J. Yu, E. Salmon, H. Wille, R. Bourayou, S. Frey, Y.-B. André, A. Mysyrowicz, R. Sauerbrey, J.-P. Wolf, and L. Wöste, Science **301**, 61 (2003); P. Rohwetter, J. Kasparian, K. Stelmaszczyk, Z. Hao, S. Henin, N. Lascoux,

W. Nakaema, Y. Petit, M. Queißer, R. Salamé, and others, Nature Photon. **4**, 451 (2010).

[6] X. Xie, J. Dai, and X. C. Zhang, Phys. Rev. Lett. **96**, 075005 (2006); K. Y. Kim, A. J. Taylor, J. H. Glownia, and G. Rodriguez, Nature Photon. **2**, 605 (2008); J. M. Manceau, A. Averchi, F. Bonaretti, D. Faccio, P. Di Trapani, A. Couairon, and S. Tzortzakis, Opt. Lett. **34**, 2165 (2009).

[7] A. Couairon and A. Mysyrowicz, Phys. Rep. **441**, 47 (2007).

[8] H. Schroeder, J. Liu, and S. Chin, Opt. Express **12**, 4768 (2004).

[9] G. Fibich, S. Eisenmann, B. Ilan, and A. Zigler, Opt. Lett. **29**, 1772 (2004); G. Méchain, A. Couairon, M. Franco, B. Prade, and A. Mysyrowicz, Phys. Rev. Lett. **93**, 035003 (2004).

[10] R. Ackermann, E. Salmon, N. Lascoux, J. Kasparian, P. Rohwetter, K. Stelmaszczyk, S. Li, A. Lindinger, L. Wöste, P. Béjot, L. Bonacina, and J.-P. Wolf, Appl. Phys. Lett. **89**, 171117 (2006); G. Heck, J. Sloss, and R. Levis, Opt. Commun. **259**, 216 (2006)

[11] D. N. Christodoulides, F. Lederer, and Y. Silberberg, Nature (London) **424**, 817 (2003);.F. Lederer, G. I. Stegeman, D. N. Christodoulides, G. Assanto, M. Segev, and Y. Silberberg, Phys. Rep. **463**, 1 (2008)

[12] D. N. Christodoulides and R. I. Joseph, Opt. Lett. **13**, 794 (1988); H. S. Eisenberg, Y. Silberberg, R. Morandotti, A. R. Boyd, and J. S. Aitchison, Phys. Rev. Lett. **81**, 3383 (1998); N. K. Efremidis, J. Hudock, D. N. Christodoulides, J. W. Fleischer, O. Cohen, and M. Segev, Phys. Rev. Lett. **91**, 213906 (2003).

[13] P. Panagiotopoulos, N. K. Efremidis, D. G. Papazoglou, A. Couairon, and S. Tzortzakis, Phys. Rev. A **82**, 061803 (2010).

[14] R. R. Gattass and E. Mazur, Nature Photon. **2**, 219 (2008); A. Szameit and S. Nolte, J. Phys. B **43**, 163001 (2010).

[15] The intensity regime is still below the modification threshold of the glass sample, and the lattice properties were confirmed to be unaffected at the end of the experiment.

[16] Y. Zhao, G. Mu, and X. Zhu, Opt. Lett. **31**, 2765 (2006).

[17] See Supplemental Material at http://link.aps.org/supplemental/10.1103/PhysRevLett.109.113905 for a detailed explanation of the numerical model used in the simulations.

[18] A. Couairon, E. Brambilla, T. Corti, D. Majus, J. De Ramirez-Gongora, and M. Kolesik, Eur. Phys. J. Special Topics **199**, 5 (2011).

[19] S. Tzortzakis, L. Berge, A. Couairon, M. Franco, B. Prade, and A. Mysyrowicz, Phys. Rev. Lett. **86**, 5470 (2001).

[20] Note that, by changing the spacing between the SF and the lattice, we observed that SFs are not significantly affected by the lattice presence down to this spacing (20 $\mu$m).